

LINEAR ATTENTION SEQUENCE PARALLELISM

Anonymous authors

Paper under double-blind review

ABSTRACT

Sequence parallelism (SP) serves as a prevalent strategy to handle long sequences that exceed the memory limit of a single device. However, for linear sequence modeling methods like linear attention, existing SP approaches do not take advantage of their right-product-first feature, resulting in sub-optimal communication efficiency and usability. In this paper, we introduce Linear Attention Sequence Parallelism (LASP), an efficient SP approach designed for linear attention-based transformer models. Specifically, we design an efficient point-to-point ring-style communication mechanism to leverage the right-product kernel trick of linear attention, which sharply decreases the communication overhead, comparing with existing SP methods. We enhance the computation efficiency of LASP by performing kernel fusion and intermediate state caching, making the implementation of LASP hardware-friendly on GPUs. Furthermore, we meticulously ensure the compatibility of sequence-level LASP with all types of batch-level data parallel methods, which is vital for distributed training on large clusters with very-long sequences. We also discuss the generalization of LASP on other linear sequence modeling methods. Extensive experiments on linear attention-based models are conducted with varying sequence lengths from 2K to 4096K. LASP scales sequence length up to 4096K on 128 GPUs, which is $8\times$ longer than existing SP methods.

1 INTRODUCTION

Recently, linear-complexity sequence modeling methods (Qin et al., 2024a; 2022a; Choromanski et al., 2022) are becoming increasingly popular due to their faster processing speed and comparable modeling performance to vanilla Softmax attention-based transformer models (Vaswani et al., 2017; Zeng et al., 2022; Touvron et al., 2023a;b). As the size of large language models (LLMs) increases and sequence lengths extend, the capacity limitations of single GPU’s memory become a significant challenge, constraining the maximum sequence length manageable by a large model. To address this, Sequence Parallelism (SP) techniques (Li et al., 2022; Korthikanti et al., 2022) are employed, which partition a long sequence into multiple sub-sequences to be processed on separate devices. However, current implementations of SP methods do not fully exploit the right-product advantages of linear-complexity attention mechanisms Qin et al. (2024b). This results in less than optimal parallelism efficiency and reduced usability on linear sequence modeling methods.

In this paper, we present Linear Attention Sequence Parallelism (LASP) approach for efficient SP on models with linear sequence modeling. Our approach takes linear attention (Katharopoulos et al., 2020) as an instance to design a sophisticated point-to-point (P2P) ring-style communication mechanism during both forward and backward among devices within a node or across multiple nodes. This design maximizes the utilization of right-product kernel tricks in linear attention, by only exchanging one single intermediate state instead of both of key and value states in other counterparts. Notably, our approach is independent of attention heads partitioning, allowing it to be applied to models with varying numbers or styles of attention heads, such as multi-head, multi-query, and grouped-query attentions. This flexibility exceeds the capabilities of existing SP methods in Megatron-LM (Shoeybi et al., 2019; Korthikanti et al., 2022) or DeepSpeed (Jacobs et al., 2023).

Our implementation of LASP incorporates system engineering optimizations such as kernel fusion and KV State caching, resulting in significantly enhanced execution efficiency. Furthermore, we have taken great care in ensuring compatibility of LASP with various (sharded) distributed data-parallel (DDP) (Li et al., 2020) training methods during the implementation, which we refer to as the data-sequence hybrid parallelism. Through extensive experiments with linear transformer models of

different parameter numbers, cluster sizes, and sequence lengths, we demonstrate the performance and efficiency of LASP when used with different DDP instances. Specifically, LASP can extend sequence length up to 4096K on 128 GPUs, which is $8\times$ longer than existing SP methods.

Our primary contributions can be summarized as follows:

- *A new SP approach called LASP that is designed for linear sequence modeling methods.* LASP is able to perform sequence-level distributed training on $8\times$ longer sequences than existing SP methods while being significantly faster.
- *Sequence length-independent communication overhead.* Our proposed P2P ring-style communication strategy leverages right-product kernel trick of linear attention to ensure that the exchanging of linear attention intermediate states is sequence length-independent.
- *GPU friendly implementation.* We optimize the execution of LASP on GPU hardware through meticulous system engineering, including kernel fusion and KV State caching.
- *Data-parallel compatibility.* LASP is compatible with all batch-level DDP methods, including PyTorch/Legacy DDP, FSDP, and ZeRO-series optimizers.

2 METHOD

2.1 PRELIMINARY

Softmax Attention. Consider the standard attention (Vaswani et al., 2017) computation with causal masking in the transformer architecture, formulated as:

$$\mathbf{O} = \text{Softmax}(\mathbf{Q}\mathbf{K}^\top / \sqrt{d} \odot \mathbf{M})\mathbf{V}, \quad (1)$$

where d denotes the hidden dimension. The matrices $\mathbf{Q}, \mathbf{K}, \mathbf{V} \in \mathbb{R}^{N \times d}$ represent query, key, and value matrices, respectively. These matrices are linear projections of the input $\mathbf{X} \in \mathbb{R}^{N \times d}$, i.e., $\mathbf{Q} = \mathbf{X}\mathbf{W}_Q$, $\mathbf{K} = \mathbf{X}\mathbf{W}_K$, $\mathbf{V} = \mathbf{X}\mathbf{W}_V$. The output matrix is denoted as $\mathbf{O} \in \mathbb{R}^{N \times d}$, and $\mathbf{M} \in \mathbb{R}^{N \times N}$ represents the causal mask matrix. The $\text{Softmax}(\cdot)$ operation introduces quadratic time complexity relative to the input sequence length N , limiting the scalability of vanilla transformers to extended input sequences.

Linear Attention. Linear attention is originally proposed in (Katharopoulos et al., 2020), with the elimination of Softmax operation (Vaswani et al., 2017). Qin et al. (2022a; 2024a) propose to replace the Softmax operation with a normalization operation $\text{Norm}(\cdot)$, which turns to

$$\mathbf{O} = \text{Norm}((\mathbf{Q}\mathbf{K}^\top \odot \mathbf{M})\mathbf{V}). \quad (2)$$

When considering bidirectional tasks, the above formulation can be simplified as $\mathbf{O} = \text{Norm}((\mathbf{Q}\mathbf{K}^\top)\mathbf{V})$. Then by performing the associativity property of matrix products, it can be mathematically equivalently transformed into a right-product version:

$$\mathbf{O} = \text{Norm}(\mathbf{Q}(\mathbf{K}^\top \mathbf{V})). \quad (3)$$

This linear attention formulation facilitates recurrent prediction with a computational complexity of $O(Nd^2)$. And the recurrent update of $\mathbf{K}^\top \mathbf{V}$ without needing to compute the entire attention matrix makes its inference efficient.

While linear complexity offers significant advantages in terms of computational efficiency and memory optimization for linear attention, it still incurs a proportional increase in computation and memory utilization on a single GPU as the sequence length N grows. This can lead to memory constraints on a single GPU, such as the 80GB limit in NVIDIA A100, for exceptionally long sequences. The challenge of achieving zero-redundancy (on sequence level) training for such long sequences using linear attention-based LLMs across GPU clusters remains an open problem. Furthermore, the complexity of addressing this issue in a casual setting further intensifies the challenge. To address this, we propose LASP as a solution for parallelizing linear attention training at the sequence level, even in a casual setting.

2.2 LASP

LASP tiles sequences over the cluster. Follow the thought-of-tiling, LASP partitions the input sequences into multiple sub-sequence chunks, distributing these chunks individually across different

108
109
110
111
112
113
114
115
116
117
118
119

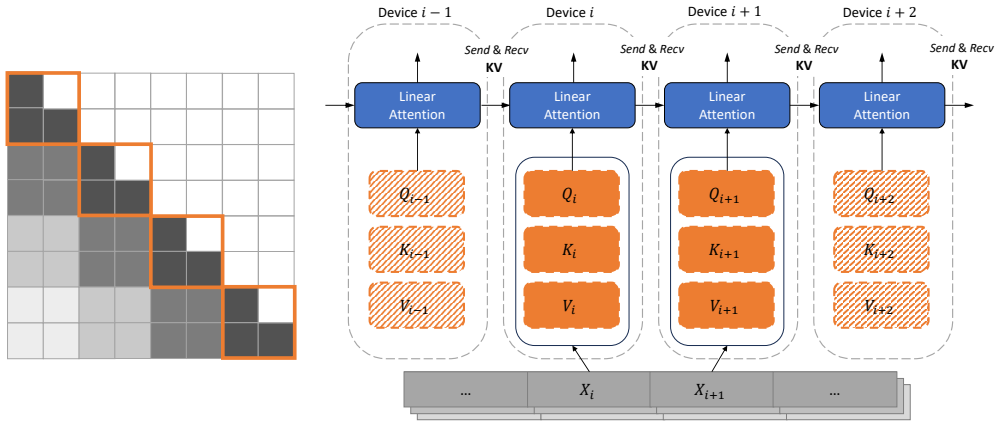
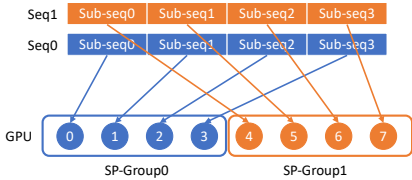


Figure 1: **Visualization of LASP.** **Left:** The chunk-level linear attention computation with a causal mask can be segmented into two categories: intra-chunk and inter-chunk computations. Intra-chunk computations, corresponding to the diagonal orange boxes) of the mask matrix, utilize traditional left-product methods. While inter-chunk computations, corresponding to the lower triangular boxes, employ efficient right-product methods for computation. **Right:** This panel illustrates the P2P communication mechanism employed by LASP. The input sequence \mathbf{X} is divided into multiple sub-sequence chunks $\{\dots, \mathbf{X}_i, \mathbf{X}_{i+1}, \dots\}$, each processed by different model instances across distinct devices. For each device i , Q_i , K_i , and V_i are computed from its respective input chunk \mathbf{X}_i . Notably, the communication operations between devices are designed to be complementary in the forward and backward passes. Specifically, in the forward pass, \mathbf{KV} matrices are sent from device i to device $(i + 1)$, and in the backward pass, \mathbf{dKV} matrices are sent back from device $(i + 1)$ to device i .

120
121
122
123
124
125
126
127
128
129
130
131
132
133
134
135
136
137
138
139
140
141
142
143
144
145
146
147



Algorithm 1 LASP Data Distribution

- 1: **Input:** An input sequence in embedding space $\mathbf{X} \in \mathbb{R}^{N \times d}$ with sequence length N and hidden dimension d , distributed world size W and sequence parallel size T .
- 2: Obtain number of sequence parallel groups $G = W/T$.
- 3: Obtain sub-sequence length (or chunk size) $C = N/T$.
- 4: Get global rank list $R = \text{get_global_rank}()$.
- 5: Obtain sequence parallel source rank list $R_{src} = \lfloor R/T \rfloor * T$.
- 6: Along sequence dimension, split \mathbf{X} into T chunks $\{\mathbf{X}_1, \mathbf{X}_2, \dots, \mathbf{X}_T\}$, of size $C \times d$ for each.
- 7: Transfer copies of data chunks $\{\mathbf{X}_1, \mathbf{X}_2, \dots, \mathbf{X}_T\}$ to GPUs with rank indices in R_{src} .
- 8: Scatter $\{\mathbf{X}_1, \mathbf{X}_2, \dots, \mathbf{X}_T\}$ from R_{src} to all ranks in respective sequence parallel groups.

Figure 2: **LASP Data Distribution.** **Left:** An example of data distribution with two input sequences and eight GPUs. **Right:** Complete data distribution algorithm.

150
151
152
153
154
155
156

GPUs. For linear attention in a casual setting, in order to fully exploit the advantage of right-product in linear attention, we categorize the attention computation for chunks into two distinct types: intra-chunks and inter-chunks. Intra-chunks involve conventional attention computation, while inter-chunks leverage the kernel tricks associated with linear attention’s right-product. Further details regarding the intricate mechanisms of LASP in data distribution, forward pass, and backward pass are expounded upon below. A visualization of LASP is presented in Fig. 1.

157
158
159
160
161

Data Distribution. LASP is designed for training long sequences on linear transformers in a distributed environment, achieved by partitioning the input data along its sequence dimension. In this situation, each GPU within the distributed environment undertakes the training of a subset of sub-sequences, which serves to diminish the large memory footprint associated with activation during the training of long sequences. Communication operations are introduced between GPUs to transmit

intermediate states. The final trained model assimilates the knowledge derived from the entirety of the long sequences.

For an input sequence of length N , we establish its embedding space representation denoted as $\mathbf{X} \in \mathbb{R}^{N \times d}$ with a feature dimension of d . In the LASP framework, \mathbf{X} is evenly partitioned into T chunks, where T is called the sequence parallel size, which must be divisible by the distributed world size W . These segmented data chunks are subsequently assigned to the respective GPUs. It is essential to note that different sequence parallel groups receive dissimilar data batches. However, within the same group, all data chunks originate from an identical batch of data. A comprehensive depiction of the data distribution process in LASP is provided in Algorithm 1.

Additionally, an illustrative example of data distribution in LASP is presented in Fig. 2, where the distributed world size is characterized by $W = 8$, the sequence parallel size by $T = 4$, the number of sequence parallel groups by $G = 2$, and the sequence parallel source rank list by $R_{src} = [0, 4]$. For the first batch SEQ0, the input sequence \mathbf{X} undergoes partitioning into T chunks $\{\mathbf{X}_1, \mathbf{X}_2, \dots, \mathbf{X}_T\}$ along the sequence dimension, subsequently transmitted to the first rank in SP-GROUP0, which corresponds to global rank 0. The data chunks on global rank 0 are then scattered to global ranks $\{0, 1, 2, 3\}$ within SP-GROUP0, where each rank only retains a single chunk. The subsequent batch SEQ1 follows a similar manner, being assigned to global ranks $\{4, 5, 6, 7\}$ within SP-GROUP1.

Forward Pass. To streamline derivations, the $\text{Norm}(\cdot)$ operator in Eq. (2) is temporarily omitted. Additionally, we consider a normal case where $W = T$, indicating $G = W/T = 1$. In this scenario, GPU with rank 0 consolidates all split sub-sequences in a batch, subsequently distributing them to all GPUs across the entire distributed world. It is noteworthy that the scenario where the sequence parallel size is not equal to world size is discussed in Sec.2.5.

We first define \mathbf{kv} and \mathbf{KV} as the intermediate memory state vector and matrix, respectively. Without loss of generality, we add λ as the decay rate in linear attention with casual masking, choosing $\lambda = 1$ yields the ordinary linear attention (Qin et al., 2024a; Sun et al., 2023). In the forward pass of linear attention computation with casual masking, the s -th output can be calculated as

$$\mathbf{o}_s^\top = \mathbf{q}_s^\top \sum_{i \leq s} \lambda^{s-i} \mathbf{k}_i \mathbf{v}_i^\top. \quad (4)$$

Rewrite in a recurrence form, we have

$$\mathbf{kv}_0 = \mathbf{0} \in \mathbb{R}^{d \times d}, \quad \mathbf{kv}_s = \lambda \mathbf{kv}_{s-1} + \mathbf{k}_s \mathbf{v}_s^\top, \quad \mathbf{o}_s^\top = \mathbf{q}_s^\top (\mathbf{kv}_s), \quad (5)$$

where

$$\mathbf{kv}_s = \sum_{i \leq s} \lambda^{s-i} \mathbf{k}_i \mathbf{v}_i^\top \quad (6)$$

is the activation memory state in the forward pass with s -th input.

In SP, given data chunk \mathbf{X}_t on rank i , the query, key and value corresponding to \mathbf{X}_t is $\mathbf{Q}_t = \mathbf{X}_t \mathbf{W}_Q$, $\mathbf{K}_t = \mathbf{X}_t \mathbf{W}_K$, $\mathbf{V}_t = \mathbf{X}_t \mathbf{W}_V$. Note that we assume $T = W$ here, their indices are thus equivalent, i.e., $t = i$. The output within the t -th chunk can be calculated as

$$\mathbf{O}_{t,\text{intra}} = [(\mathbf{Q}_t \mathbf{K}_t^\top) \odot \mathbf{M}] \mathbf{V}_t. \quad (7)$$

Algorithm 2 LASP Forward Pass

- 1: **Input:** input sequence in embedding space $\mathbf{X} \in \mathbb{R}^{N \times d}$ with sequence length N and hidden dimension d , distributed world size W , sequence parallel size $T = W$, decay rate $\lambda \in \mathbb{R}^+$.
 - 2: Distribute input sequence \mathbf{X} according to Algorithm 1.
 - 3: Obtain sub-sequence length (or chunk size) $C = N/T$.
 - 4: Initialize mask $\mathbf{M} \in \mathbb{R}^{C \times C}$, where $M_{ij} = \lambda^{i-j}$, if $i \geq j$, else $M_{ij} = 0$.
 - 5: Initialize $\mathbf{\Lambda} = \text{diag}\{\lambda, \lambda^2, \dots, \lambda^C\} \in \mathbb{R}^{C \times C}$.
 - 6: Initialize activation state $\mathbf{KV} = \mathbf{0} \in \mathbb{R}^{d \times d}$.
 - 7: **for** chunk $t \in \{1, \dots, T\}$ at rank $i \in \{1, \dots, W\}$ in parallel **do**
 - 8: Calculate $\mathbf{Q}_t = \mathbf{X}_t \mathbf{W}_Q$, $\mathbf{K}_t = \mathbf{X}_t \mathbf{W}_K$, $\mathbf{V}_t = \mathbf{X}_t \mathbf{W}_V$ according to its own data chunk, of size $C \times d$ for each.
 - 9: Compute $\mathbf{O}_{t,\text{intra}} = [(\mathbf{Q}_t \mathbf{K}_t^\top) \odot \mathbf{M}] \mathbf{V}_t$.
 - 10: **end for**
 - 11: **for** chunk $t \in \{1, \dots, T\}$ at rank $i \in \{1, \dots, W\}$ **do**
 - 12: Recv activation \mathbf{KV}_{t-1} from rank $(i-1)$.
 - 13: Save \mathbf{KV}_{t-1} as \mathbf{KV}_i for backward computation.
 - 14: Compute $\mathbf{O}_{t,\text{inter}} = \mathbf{\Lambda} \mathbf{Q}_t \mathbf{KV}_{t-1}$.
 - 15: Compute $\mathbf{O}_t = \mathbf{O}_{t,\text{intra}} + \mathbf{O}_{t,\text{inter}}$.
 - 16: Update $\mathbf{KV}_t = \lambda^C \mathbf{KV}_{t-1} + (\lambda^C \mathbf{\Lambda}^{-1} \mathbf{K}_t)^\top \mathbf{V}_t$.
 - 17: Send activation \mathbf{KV}_t to rank $(i+1)$.
 - 18: **end for**
 - 19: return $\mathbf{O} = [\mathbf{O}_t]$, with $t \in \{1, \dots, T\}$.
-

The intra-chunk computation has no dependencies with other chunks on other GPUs, so it can be calculated parallelized on all ranks in the distributed world. However, this result does not consider the impact of the previous $1 \sim (t-1)$ chunks on the t -th chunk, which is called an inter-chunk. To calculate inter-chunk, let us rearrange Eq. (4) as

$$\mathbf{o}_{s+C}^\top = \mathbf{q}_{s+C}^\top \sum_{i \leq s+C} \lambda^{s+C-i} \mathbf{k}_i \mathbf{v}_i^\top = \mathbf{q}_{s+C}^\top \sum_{i=C+1}^{C+s} \lambda^{s+C-i} \mathbf{k}_i \mathbf{v}_i^\top + \lambda^s \mathbf{q}_{s+C}^\top \sum_{i \leq C} \lambda^{C-i} \mathbf{k}_i \mathbf{v}_i^\top. \quad (8)$$

The resulted first part in Eq. (8) corresponds to the computation on previous chunks, and the second part corresponds to the computation on the current chunk. In SP, Eq. (8) can be rewritten in the chunk form as

$$\mathbf{O}_{t,\text{inter}} = \Lambda \mathbf{Q}_t \mathbf{K} \mathbf{V}_{t-1}, \quad (9)$$

where $\mathbf{K} \mathbf{V}_t = \mathbf{k} \mathbf{v}_{tC}$. Note that the calculation of the inter-chunk for the t -th chunk depends on the activation state of previous $(t-1)$ chunk, *i.e.*, $\mathbf{K} \mathbf{V}_{t-1}$, which is calculated on rank $(i-1)$. Thus a P2P communication operation `Recv` should be performed to pull $\mathbf{K} \mathbf{V}_{t-1}$ from rank $(i-1)$ to rank i . Then the activation state $\mathbf{K} \mathbf{V}_t$ should be updated for subsequent inter-chunk attention computation at $(t+1)$ -th chunk. The update rule of $\mathbf{K} \mathbf{V}_t$ at t -th chunk is

$$\begin{aligned} \mathbf{K} \mathbf{V}_t &= \sum_{s \leq tC} \lambda^{tC-s} \mathbf{k}_s \mathbf{v}_s^\top = \lambda^C \sum_{s \leq (t-1)C} \lambda^{(t-1)C-s} \mathbf{k}_s \mathbf{v}_s^\top + \sum_{s=(t-1)C+1}^{tC} \lambda^{tC-s} \mathbf{k}_s \mathbf{v}_s^\top \\ &= \lambda^C \mathbf{K} \mathbf{V}_{t-1} + (\text{diag}\{\lambda^{C-1}, \dots, 1\} \mathbf{K}_t)^\top \mathbf{V}_t = \lambda^C \mathbf{K} \mathbf{V}_{t-1} + (\lambda^C \Lambda^{-1} \mathbf{K}_t)^\top \mathbf{V}_t. \end{aligned} \quad (10)$$

In correspondence to the preceding `Recv` operation, another P2P communication operation `Send` is executed to transmit the acquired $\mathbf{K} \mathbf{V}_t$ in Eq. (10) to the subsequent rank $(i+1)$ for its inter-chunk computation.

It is noteworthy that in the backward pass, the t -th chunk necessitates $\mathbf{K} \mathbf{V}_{t-1}$ as activation to calculate gradients. To minimize communication operations, we cache $\mathbf{K} \mathbf{V}_{t-1}$ on High-Bandwidth Memory (HBM) to accelerate computation. Integrating both the intra and inter parts, the final forward output is as follows:

$$\mathbf{O}_t = \mathbf{O}_{t,\text{intra}} + \mathbf{O}_{t,\text{inter}} \quad (11)$$

We present the complete forward pass of LASP with $W = T$ in Algorithm 2.

Backward Pass. For the backward pass, given $\mathbf{d}\mathbf{o}_s$, we have (Katharopoulos et al., 2020)

$$\begin{aligned} \mathbf{d}\mathbf{q}_s^\top &= \mathbf{d}\mathbf{o}_s^\top \mathbf{k} \mathbf{v}_s^\top \in \mathbb{R}^{1 \times d}, \quad \mathbf{d}\mathbf{k}_s^\top = \mathbf{v}_s^\top \mathbf{d}\mathbf{k} \mathbf{v}_s^\top \in \mathbb{R}^{1 \times d}, \\ \mathbf{d}\mathbf{v}_s^\top &= \mathbf{k}_s^\top \mathbf{d}\mathbf{k} \mathbf{v}_s \in \mathbb{R}^{1 \times d}, \quad \mathbf{d}\mathbf{k} \mathbf{v}_s = \sum_{i \geq s} \lambda^{i-s} \mathbf{q}_i \mathbf{d}\mathbf{o}_i^\top \in \mathbb{R}^{d \times d}. \end{aligned} \quad (12)$$

By writing $\mathbf{d}\mathbf{k} \mathbf{v}_s$ in a recursive form, we have

$$\mathbf{d}\mathbf{k} \mathbf{v}_{n+1} = 0 \in \mathbb{R}^{d \times d}, \quad \mathbf{d}\mathbf{k} \mathbf{v}_{s-1} = \lambda \mathbf{d}\mathbf{k} \mathbf{v}_s + \mathbf{q}_{s-1} \mathbf{d}\mathbf{o}_{s-1}^\top. \quad (13)$$

In SP, we have $\{\mathbf{Q}_t, \mathbf{K}_t, \mathbf{V}_t, \mathbf{O}_t, \mathbf{d}\mathbf{O}_t\}$ which corresponds to the t -th sub-sequence chunk on rank i , where $t \in \{1, \dots, T\}$ and $i \in \{1, \dots, W\}$. Same with the forward pass, the following derivations assume $t = i, T = W$.

We first calculate $\mathbf{d}\mathbf{Q}$ with respect to the t -th data chunk, which yields:

$$\mathbf{d}\mathbf{Q}_{t,\text{intra}} = [(\mathbf{d}\mathbf{O}_t \mathbf{V}_t^\top) \odot \mathbf{M}] \mathbf{K}_t. \quad (14)$$

Since the computation of $\mathbf{d}\mathbf{Q}_{t,\text{intra}}$ is independent, its calculation can be parallelized on all GPUs. While the calculation of $\mathbf{d}\mathbf{Q}_{t,\text{inter}}$ reflects the inter-dependence of chunks 1 to $t-1$ on chunk t . In order to compute the inter part, we transform Eq. (12) as

$$\mathbf{d}\mathbf{q}_{s+C}^\top = \mathbf{d}\mathbf{o}_{s+C}^\top \sum_{i \leq s+C} \lambda^{s+C-i} \mathbf{v}_i \mathbf{k}_i^\top = \mathbf{d}\mathbf{o}_{s+C}^\top \sum_{i=C+1}^{C+s} \lambda^{s+C-i} \mathbf{v}_i \mathbf{k}_i^\top + \lambda^s \mathbf{d}\mathbf{o}_{s+C}^\top \sum_{i \leq C} \lambda^{C-i} \mathbf{v}_i \mathbf{k}_i^\top. \quad (15)$$

The first part in Eq. (15) corresponds to the intra-chunk, while the second part corresponds to the inter-chunk. In SP, we can calculate $\mathbf{dQ}_{t,\text{inter}}$ as

$$\mathbf{dQ}_{t,\text{inter}} = \Lambda \mathbf{dO}_t \mathbf{KV}_{t-1}^\top. \quad (16)$$

Note that \mathbf{KV}_t has already been computed and cached during the forward pass, so no communication is required here to obtain \mathbf{KV}_t . Benefit from the \mathbf{KV} state caching, the calculation of $\mathbf{dQ}_{t,\text{inter}}$ can also be executed in parallel.

Next, \mathbf{dK} within the t -th chunk can be calculated in parallel as

$$\mathbf{dK}_{t,\text{intra}} = [(\mathbf{dO}_t \mathbf{V}_t^\top) \odot \mathbf{M}]^\top \mathbf{Q}_t. \quad (17)$$

Then we transform Eq. (12) as

$$\mathbf{dk}_s^\top = \mathbf{v}_s^\top \sum_{i \geq s} \lambda^{i-s} \mathbf{do}_i \mathbf{q}_i^\top = \mathbf{v}_s^\top \sum_{i=s}^C \lambda^{i-s} \mathbf{do}_i \mathbf{q}_i^\top + \lambda^{C-s} \mathbf{v}_s^\top \sum_{i \geq C+1} \lambda^{i-C} \mathbf{do}_i \mathbf{q}_i^\top, \quad (18)$$

where the term before plus sign corresponds to the intra-chunk, and the term after plus sign corresponds to the inter-chunk. The above equation can be rewritten in terms of chunks as follow:

$$\mathbf{dK}_{t,\text{inter}} = \lambda^C \Lambda^{-1} \mathbf{V}_t \mathbf{dKV}_{t+1}^\top. \quad (19)$$

Here a `Recv` operation is required here to pull \mathbf{dKV}_{t+1} from the $(t+1)$ -th chunk. Then in order to compute \mathbf{dKV} for the $(t-1)$ -th chunk, \mathbf{dKV} should be updated as:

$$\begin{aligned} \mathbf{dKV}_t &= \sum_{s > tC} \lambda^{s-tC} \mathbf{q}_s \mathbf{do}_s^\top = \lambda^C \sum_{s > (t+1)C} \lambda^{s-(t+1)C} \mathbf{q}_s^\top \mathbf{do}_s + \sum_{s=tC+1}^{(t+1)C} \lambda^{s-tC} \mathbf{q}_s \mathbf{do}_s^\top \\ &= \lambda^C \mathbf{dKV}_{t+1} + (\Lambda \mathbf{Q}_t)^\top \mathbf{dO}_t. \end{aligned} \quad (20)$$

Then a `Send` operation is performed to push \mathbf{dKV}_t to rank $(i-1)$. Finally, for \mathbf{dV} , its intra part can be calculated as $\mathbf{dV}_{t,\text{intra}} = [(\mathbf{Q}_t \mathbf{K}_t^\top) \odot \mathbf{M}]^\top \mathbf{dO}_t$. Again we transform Eq. (12) as:

$$\mathbf{dv}_s^\top = \mathbf{k}_s^\top \sum_{i \geq s} \lambda^{i-s} \mathbf{q}_i \mathbf{do}_i^\top = \mathbf{k}_s^\top \sum_{i=s}^C \lambda^{i-s} \mathbf{q}_i \mathbf{do}_i^\top + \lambda^{C-s} \mathbf{k}_s^\top \sum_{i \geq C+1} \lambda^{i-C} \mathbf{q}_i \mathbf{do}_i^\top. \quad (21)$$

The first and second terms corresponds to the computation of the intra- and inter-chunks, respectively. In SP, $\mathbf{dV}_{t,\text{inter}}$ can be calculated as:

$$\mathbf{dV}_{t,\text{inter}} = \lambda^C \Lambda^{-1} \mathbf{K}_t \mathbf{dKV}_{t+1}. \quad (22)$$

Combine the intra and inter part, we obtain the final results of \mathbf{dQ}_t , \mathbf{dK}_t and \mathbf{dV}_t :

$$\mathbf{dQ}_t = \mathbf{dQ}_{t,\text{intra}} + \mathbf{dQ}_{t,\text{inter}}, \mathbf{dK}_t = \mathbf{dK}_{t,\text{intra}} + \mathbf{dK}_{t,\text{inter}}, \mathbf{dV}_t = \mathbf{dV}_{t,\text{intra}} + \mathbf{dV}_{t,\text{inter}}. \quad (23)$$

We provide the complete backward pass of LASP in Algorithm 3 in Appendix A.1.

2.3 COMPARISON

In LASP, it is important to note that the forward pass requires communication for the $\mathbf{KV} \in \mathbb{R}^{d \times d}$ state in each linear attention module layer. The communication volume is determined by Bd^2/h , where B is the batch size and h is the number of heads. In comparison, Ring Attention also adopts P2P ring-style communication on states $\mathbf{K}, \mathbf{V} \in \mathbb{R}^{V \times d}$, which results a communication volume of BNd/h . SP in Megatron-LM utilizes all-gather operations twice after two layer normalization layers within each transformer layer, and a reduce-scatter operation after the attention and Feedforward Neural Network (FFN) layers. This results in a communication volume of $2BNd + 4BNd/T$. DeepSpeed uses all-to-all collective communication (Thakur et al., 2005) for input $\mathbf{Q}, \mathbf{K}, \mathbf{V}$, and output \mathbf{O} of each attention module layer, resulting in a communication volume of $4BNd/T$.

Table 1 displays a comparison of communication volumes across three frameworks. d/h is the head dimension which is set at 128 as usual (Lan et al., 2020). In practical applications where $N/T \geq 32$, LASP is able to achieve the lowest theoretical communication volume. Furthermore, the communication volume of LASP is not impacted by changes in sequence length N or sub-sequence length C , which is a huge advantage for SP with very-long sequences across large clusters.

Table 1: **Communication Volume Comparison.** Simplified Formulation: we eliminate the common factors Bd for ease of comparison.

Method	Full Formulation	Simplified Formulation
LASP	Bd^2/h	d/h
Ring Attention	$2BNd/h$	$2N/h$
DeepSpeed-Ulysses	$4BNd/T$	$4N/T$
Megatron-SP	$2BNd + 4BNd/T$	$2N + 4N/T$

It is worth to note that, although Ring Attention and LASP both use P2P ring-style communication, they have differences lie in both communication and computation sides. *Communication*: In both forward and backward, Ring Attention involves communicating two states $\mathbf{K}, \mathbf{V} \in \mathbb{R}^{V \times d}$. In contrast, LASP only communicates one single state $\mathbf{KV} \in \mathbb{R}^{d \times d}$, which does not depend on the sequence length. LASP has a lower theoretical communication complexity. This makes LASP more efficient, especially in environments with slower interconnects where the communication-computation overlap may not be optimal. *Computation*: Ring Attention is specifically designed for standard attention, utilizing a left-product manner, i.e., $((\mathbf{Q}\mathbf{K}^T)\mathbf{V})$. On the other hand, LASP is specifically tailored for linear attention-like sequence modeling methods, which leverages the right-product kernel trick $(\mathbf{Q}(\mathbf{K}^T\mathbf{V}))$ to achieve linear-time complexity.

2.4 SYSTEM ENGINEERING OPTIMIZATION

Kernel Fusion. To improve the efficiency of LASP on GPU, we perform kernel fusion in both the intra-chunk and inter-chunk computations, and also fused the updates of \mathbf{KV} and $d\mathbf{KV}$ into the intra-chunk and inter-chunk computations.

KV State Caching. To avoid recomputing activation \mathbf{KV} during the backward pass, we choose to store it in the HBM of the GPU right after computing it in the forward pass. During the subsequent backward pass, LASP directly accesses \mathbf{KV} for use. It is important to note that the size of the \mathbf{KV} activation cached in HBM is $d \times d$, which is not affected by the sequence length N . When the input sequence length N is exceptionally large, the memory usage of \mathbf{KV} becomes negligible.

2.5 HYBRID PARALLELISM

Data-Sequence Hybrid Parallelism. As illustrated in Fig. 2, LASP allows for the specification of a smaller sequence parallel size that is divisible by the distributed world size. This configuration results in the input data being split along both the batch and sequence dimensions, which is a type of hybrid parallelism called data-sequence hybrid parallelism. The ZeRO-series optimizers (Rajbhandari et al., 2020) in DeepSpeed and FSDP (Zhao et al., 2023) in PyTorch propose to distribute model states, which include optimizer states, gradients, and model parameters, across all GPUs within the distributed environment. As variants of data parallelism, these techniques seamlessly align with LASP. Furthermore, their focus on minimizing the memory of model states complements LASP’s objective of reducing activation memory on each GPU. By integrating these techniques, the training of large models handling long sequence lengths is rendered more practical.

Compatibility with Tensor Parallelism and Pipeline Parallelism. LASP supports both tensor parallelism (TP) and pipeline parallelism (PP). In the context of PP, as exemplified by the GPipe (Kim et al., 2020) scheduling method, the model is initially partitioned across multiple devices, with each device holding a segment of the model. Data within a mini-batch is then divided into micro-batches, which are sequentially fed into the device containing the first segment. Each device processes its micro-batch and forwards the output to the next device in the sequence, simultaneously preparing to receive and process the subsequent micro-batch from the preceding device. This method of pipelining inputs effectively minimizes device idle times. When LASP is integrated with PP, micro-batches are substituted with sub-sequences derived from a mini-batch. Unlike standard PP, each device retains the intermediate states (\mathbf{KV} in the forward pass and $d\mathbf{KV}$ in the backward pass) locally, rather than transmitting them to the next device as typically done in LASP alone. For TP, the integration with LASP is fluid. Linear attention layers utilize TP to segment matrix operations across both intra-chunk

and inter-chunk computations, whereas the handling of MLP layers under TP remains unchanged. The experiment tests on hybrid of LASP, DP, TP and SP will be conducted in the future work.

3 RELATED WORK

Linear Attention. Linear Transformer models bypass the use of Softmax attention by adopting various approximation methods (Katharopoulos et al., 2020; Choromanski et al., 2020; Peng et al., 2021; Qin et al., 2022b;a) instead. The central concept involves using the "kernel trick" to speed up the calculation of the attention matrix, specifically by multiplying keys and values before tackling the computationally intensive $n \times n$ matrix multiplication. For instance, Katharopoulos et al. (2020) use $1 + \text{elu}$ activation function, Qin et al. (2022b) utilizes the cosine function to imitate Softmax characteristics, and Choromanski et al. (2020); Zheng et al. (2022; 2023) leverage sampling techniques to closely replicate the Softmax process are all strategies employed to achieve this.

Memory-Efficient Attention. Rabe & Staats (2021) first employs the *online Softmax* technique to efficiently compute numerically stable attention scores sequentially, resulting in a linear memory for attention, yet still needs quadratic time complexity. While FlashAttention (Dao et al., 2022; Dao, 2023) employs tiling to minimize the number of memory reads/writes between GPU's high bandwidth memory (HBM) and on-chip SRAM to reduce time and memory in the training process, PagedAttention (Kwon et al., 2023) optimizes the utilization of the KV cache memory by reducing waste and enabling adaptable sharing among batched requests during inference. Ring Attention (Liu et al., 2023) reduces memory requirements for Transformer models when handling long sequences by distributing sequences across multiple devices and overlapping the communication of key-value blocks with blockwise attention computation.

Sequence Parallelism. SP as a widely used method to train long sequences has been integrated into many large model training frameworks, including Megatron-LM, DeepSpeed, and Colossal-AI. Megatron-LM (Shoeybi et al., 2019) implements SP along with model (tensor) parallelism (MP) to perform large matrix multiplications on GPUs. However, MP partitions the attention heads, which limits the maximum parallelism degree to be less than the number of attention heads. DeepSpeed-Ulysses (Jacobs et al., 2023) uses an all-to-all communication primitive to reduce communication volume, but also partitions attention heads and faces similar issues as Megatron-LM.

4 EXPERIMENTS

We evaluate LASP on two representative linear attention-based models: TransNormerLLM (TNL) (Qin et al., 2024a) and Linear Transformer (Katharopoulos et al., 2020). TNL is the latest large language model purely built upon linear attention, while Linear Transformer is a classical linear transformer model recognized in the community. Our assessment focuses on three key areas: 1) the ability of LASP to scale up sequence length on scaling-out GPUs, 2) the convergence when using LASP, and 3) speed evaluation when using LASP and its comparison with other SP methods. No activation checkpointing (AC) (Korthikanti et al., 2022) techniques are used in following experiments to reduce activation memory, except experiments in Section A.5.3. This is because although the adoption of AC will further enables longer sequence lengths, it will cover up the ability of our sequence parallel method LASP. All experiments are conducted on a GPU cluster equipped with 128x A100 80G GPUs. Our implementation is built on Metaseq (Zhang et al., 2022), a PyTorch-based sequence modeling framework with FairScale (FairScale authors, 2021) integrated. For more details of hardware and software, and experimental setup, see Appendix A.2 & A.3.

Note that when implement other SP methods (e.g., Ring Attention, DeepSpeed-ulysses and Megatron-SP) on linear attention instances for the purpose of comparison, we do not use the right-product kernel trick. We maintain the use of each method's original communication primitives and computational manners as they originally proposed for standard softmax attention.

4.1 SCALABILITY AND SPEED COMPARISON

The scalability results regarding throughput and memory usage with varying sequence lengths and number of GPUs are illustrated in Fig. 3. By using LASP, we successfully scale the sequence length up to 4096K using the FSDP backend and 2048K with the DDP backend on a TNL model with 1B parameters, on 128 GPUs. We keep using a fixed batch size of 1 to thoroughly assess the performance of LASP across a range of sequence lengths, from a typical 2K to an exceptionally long 4096K. By

432
433
434
435
436
437
438
439
440
441

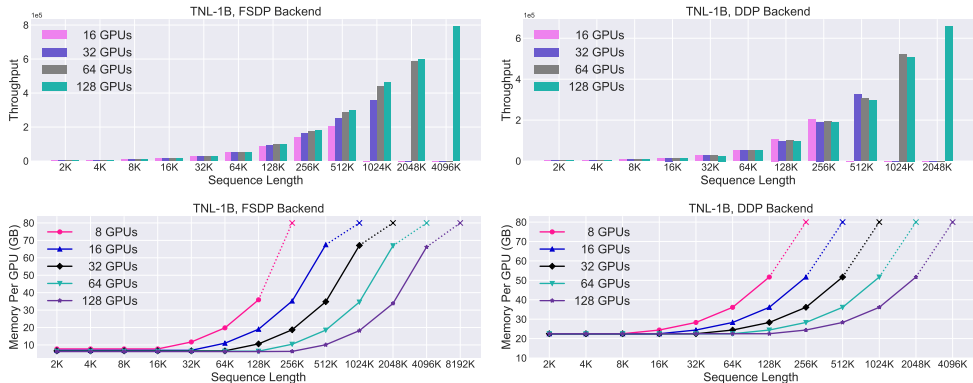


Figure 3: **Scalability Evaluation of LASP on Throughput (tokens/sec) and Memory Usage.** Left: Integration of LASP with FSDP backend; Right: Integration of LASP with DDP backend. The TNL-1B model is used, with a batch size of 1 across up to 128x A100 80GB GPUs. The sign "x" with a dotted line represents occurring an Out of Memory (OOM).

442
443
444
445
446
447
448
449
450
451

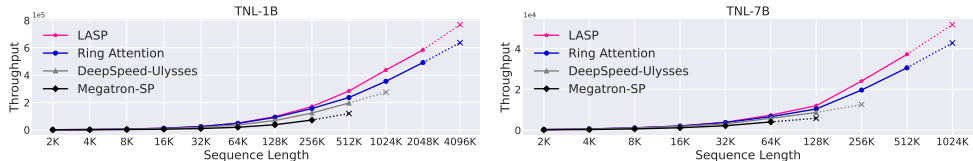


Figure 4: **Speed Comparison (tokens/sec) of LASP Against Ring Attention, DeepSpeed-Ulysses and Megatron-SP.** The sign "x" with a dotted line represents occurring an Out of Memory (OOM). The evaluation utilizes the TNL-1B and 7B models with a batch size of 1 on 64x A100 80GB GPUs. The parallelism size for these three methods is configured to 64.

452
453
454
455
456
457
458
459
460
461
462
463
464
465
466
467
468
469
470
471
472
473
474
475
476
477

keeping the batch size constant at 1, we ensure that the experiment results are directly comparable, with only the sequence length varying.

Importantly, the implementation of LASP allows for a linear increase in the maximum sequence length capacity, directly proportional (linear) to the number of GPUs used. For instance, a sequence length of 512K can be trained using 16 GPUs, while 64 GPUs (4x) has is able to train 2048K (4x) sequence length. Enabling LASP maintains a high throughput level even with more GPUs used. Furthermore, LASP demonstrates consistent scalability performance under both the FSDP and DDP backends. For more quantitative scalability results of LASP, see Table 4 in Appendix A.5.

We furthermore conducted a comparison of SP on TNL 1B and 7B models against existing SP methods: Ring Attention (Liu et al., 2023), DeepSpeed-Ulysses (Jacobs et al., 2023) and Megatron-SP (Korthikanti et al., 2022). All results presented in Fig. 4 are obtained on 64 GPUs. LASP demonstrates a notable enhancement in throughput for linear attention, primarily due to its efficient communication design that facilitates the exchange of linear attention intermediate states. Specifically, LASP outperforms all counterparts in terms of throughput at 256K sequence length on 1B model, with the performance gap widening as the sequence length increases. Additionally, system optimizations like kernel fusion and KV State caching enable LASP to support the longest sequence lengths within the same cluster, achieving 2048K for the 1B model and 512K for the 7B model.

4.2 CONVERGENCE

478
479
480
481
482
483
484

Table 2 presents the convergence results of two linear attention based models: TNL (Qin et al., 2024a) and Linear Transformer (Katharopoulos et al., 2020), and one transformer model (LLaMA (Touvron et al., 2023a;b)) with Softmax attention, evaluated on an epoch-by-epoch basis. The experiments were conducted using the same training corpus: the Pile (Gao et al., 2020). Both linear models has 0.4B parameters, demonstrated consistent loss values when training with and without LASP. All experiments undergoes 50K steps. The uniform loss convergence across various DDP backends demonstrates that LASP does not negatively affect model convergence.

485

For ablation studies on system engineering optimization techniques and activation checkpointing, and evaluation results on downstream tasks, please refer to more results in Appendix A.5.

Table 2: **Convergence Performance of LASP.** All experiments use 8x A100 80G GPUs, sequence length of 16K, and batch size of 1. The results cover various DDP backends in conjunction with LASP. We explore the performance of two linear attention models: TransNormerLLM (TNL) and Linear Transformer, and one transformer model (LLaMA) with Softmax attention, all with 0.4B parameters, across 50K updates. We compare the loss values (lower is better) with and without LASP.

Model	Parameters	Method	Loss	Method	Loss
Transformer	0.4B	DDP	3.727	\	\
TNL (Qin et al., 2024a)	0.4B	DDP	3.719	LASP + DDP	3.715
		Legacy DDP	3.709	LASP + Legacy DDP	3.705
		FSDP	3.717	LASP + FSDP	3.714
		ZeRO-1	3.653	LASP + ZeRO-1	3.653
		ZeRO-2	3.655	LASP + ZeRO-2	3.649
		ZeRO-3	3.656	LASP + ZeRO-3	3.649
Linear Transformer (Katharopoulos et al., 2020)	0.4B	DDP	5.419	LASP + DDP	5.408
		Legacy DDP	5.425	LASP + Legacy DDP	5.413
		FSDP	5.428	LASP + FSDP	5.441
		ZeRO-1	5.114	LASP + ZeRO-1	5.118
		ZeRO-2	5.105	LASP + ZeRO-2	5.120
		ZeRO-3	5.110	LASP + ZeRO-3	5.123

5 DISCUSSION

Linear-complexity sequence modeling methods are emerging as important alternatives to traditional transformers (using Softmax attention) for next-generation foundational models due to their significantly faster training and inference times, coupled with performance that rivals conventional approaches. Recently, the AI community has seen a rapid development of novel linear-complexity models, gaining considerable interest. Examples include linear attention models such as TransNormerLLM, state space models (SSM) like Mamba and Jamba, and linear RNN models including RWKV, HGRN, and Griffin. We contend that the LASP design can be seamlessly integrated into most linear-complexity models. To underscore LASP’s generalization, we use a generalized form of linear attention in Appendix A.4 (Qin et al., 2024b), demonstrating that the majority of linear-complexity models can be accommodated within this broad framework.

6 CONCLUSION

We presented LASP to effectively address the limitations of existing SP methods on linear-complexity sequence modeling methods by leveraging their right-product features, which significantly enhanced communication and parallelism efficiency. Through the design of an efficient P2P ring-style communication mechanism and elaborated engineering optimizations including kernel fusion and KV state caching, LASP achieved a notable reduction in communication traffic and improved hardware utilization on GPU clusters. Compatibility with all types of batch-level DDP methods ensured the practicability of LASP for large-scale distributed training with very-long sequences. Our experiments highlighted the advantages of LASP on scalability, speed, memory usage and convergence performance. In specific experimental setup, LASP achieves significant faster sequence-level distributed training speed on a maximum $8\times$ longer sequence length than the out-of-the-box SP methods.

540 BROADER IMPACT

541

542 This work represents a notable advancement in artificial intelligence and machine learning, particularly
 543 in improving the efficiency and scalability of linear attention-based models. LASP-2 enables the
 544 processing of much longer sequences compared to existing methods while significantly accelerating
 545 computation, making it highly beneficial for tasks like natural language understanding, genomic
 546 sequence analysis, and time-series forecasting. However, the enhanced capabilities and efficiency
 547 introduced by LASP-2 also raise ethical and societal considerations, such as the potential for misuse
 548 in generating persuasive but misleading content or in surveillance applications. Nevertheless, the
 549 contributions of LASP-2 to reducing computational overhead and energy consumption in training
 550 large models may also bring positive environmental impacts.

551

552 REFERENCES

553

554 Krzysztof Choromanski, Valerii Likhoshesterov, David Dohan, Xingyou Song, Andreea Gane, Tamás
 555 Sarlós, Peter Hawkins, Jared Davis, Afroz Mohiuddin, Lukasz Kaiser, David Belanger, Lucy J.
 556 Colwell, and Adrian Weller. Rethinking attention with performers. *ArXiv*, abs/2009.14794, 2020.

557 Krzysztof Choromanski, Valerii Likhoshesterov, David Dohan, Xingyou Song, Andreea Gane, Tamas
 558 Sarlos, Peter Hawkins, Jared Davis, Afroz Mohiuddin, Lukasz Kaiser, David Belanger, Lucy
 559 Colwell, and Adrian Weller. Rethinking attention with performers, 2022.

560 Tri Dao. Flashattention-2: Faster attention with better parallelism and work partitioning. *arXiv*
 561 *preprint arXiv:2307.08691*, 2023.

562 Tri Dao, Dan Fu, Stefano Ermon, Atri Rudra, and Christopher Ré. Flashattention: Fast and memory-
 563 efficient exact attention with io-awareness. *Advances in Neural Information Processing Systems*,
 564 35:16344–16359, 2022.

565 FairScale authors. Fairscale: A general purpose modular pytorch library for high performance and
 566 large scale training. <https://github.com/facebookresearch/fairscale>, 2021.

567 Leo Gao, Stella Biderman, Sid Black, Laurence Golding, Travis Hoppe, Charles Foster, Jason Phang,
 568 Horace He, Anish Thite, Noa Nabeshima, Shawn Presser, and Connor Leahy. The pile: An 800gb
 569 dataset of diverse text for language modeling, 2020.

570 Albert Gu and Tri Dao. Mamba: Linear-time sequence modeling with selective state spaces. *arXiv*
 571 *preprint arXiv:2312.00752*, 2023.

572 Albert Gu, Karan Goel, and Christopher Ré. Efficiently modeling long sequences with structured
 573 state spaces. In *The International Conference on Learning Representations (ICLR)*, 2022.

574 Ankit Gupta, Albert Gu, and Jonathan Berant. Diagonal state spaces are as effective as structured
 575 state spaces, 2022.

576 Sam Ade Jacobs, Masahiro Tanaka, Chengming Zhang, Minjia Zhang, Shuaiwen Leon Song, Samyam
 577 Rajbhandari, and Yuxiong He. DeepSpeed Ulysses: System optimizations for enabling training of
 578 extreme long sequence transformer models, 2023.

579 Angelos Katharopoulos, Apoorv Vyas, Nikolaos Pappas, and François Fleuret. Transformers are rNNS:
 580 Fast autoregressive transformers with linear attention. In *International Conference on Machine*
 581 *Learning*, pp. 5156–5165. PMLR, 2020.

582 Tobias Katsch. Gateloop: Fully data-controlled linear recurrence for sequence modeling. *arXiv*
 583 *preprint arXiv:2311.01927*, 2023.

584 Chiheon Kim, Heungsub Lee, Myungryoung Jeong, Woonhyuk Baek, Boogyeon Yoon, Ildoo Kim,
 585 Sungbin Lim, and Sungwoong Kim. torchpipe: On-the-fly pipeline parallelism for training giant
 586 models. 2020.

587 Vijay Korthikanti, Jared Casper, Sangkug Lym, Lawrence McAfee, Michael Andersch, Mohammad
 588 Shoeybi, and Bryan Catanzaro. Reducing activation recomputation in large transformer models,
 589 2022.

593

- 594 Woosuk Kwon, Zhuohan Li, Siyuan Zhuang, Ying Sheng, Lianmin Zheng, Cody Hao Yu, Joseph E.
595 Gonzalez, Hao Zhang, and Ion Stoica. Efficient memory management for large language model
596 serving with pagedattention, 2023.
597
- 598 Zhenzhong Lan, Mingda Chen, Sebastian Goodman, Kevin Gimpel, Piyush Sharma, and Radu
599 Soricut. Albert: A lite bert for self-supervised learning of language representations, 2020.
600
- 601 Shen Li, Yanli Zhao, Rohan Varma, Omkar Salpekar, Pieter Noordhuis, Teng Li, Adam Paszke, Jeff
602 Smith, Brian Vaughan, Pritam Damania, and Soumith Chintala. Pytorch distributed: Experiences
603 on accelerating data parallel training, 2020.
- 604 Shenggui Li, Fuzhao Xue, Chaitanya Baranwal, Yongbin Li, and Yang You. Sequence parallelism:
605 Long sequence training from system perspective, 2022.
606
- 607 Hao Liu, Matei Zaharia, and Pieter Abbeel. Ring attention with blockwise transformers for near-
608 infinite context, 2023.
- 609 Huanru Henry Mao. Fine-tuning pre-trained transformers into decaying fast weights. In *Proceedings*
610 *of the 2022 Conference on Empirical Methods in Natural Language Processing*, pp. 10236–10242,
611 Abu Dhabi, United Arab Emirates, December 2022. Association for Computational Linguistics.
612 URL <https://aclanthology.org/2022.emnlp-main.697>.
613
- 614 Eric Martin and Chris Cundy. Parallelizing linear recurrent neural nets over sequence length. In
615 *International Conference on Learning Representations*, 2018. URL <https://openreview.net/forum?id=HyUNwulC->.
616
- 617 Bo Peng, Eric Alcaide, Quentin Anthony, Alon Albalak, Samuel Arcadinho, Stella Biderman, Huanqi
618 Cao, Xin Cheng, Michael Chung, Leon Derczynski, Xingjian Du, Matteo Grella, Kranthi Gv,
619 Xuzheng He, Haowen Hou, Przemyslaw Kazienko, Jan Kocon, Jiaming Kong, Bartłomiej Koptyra,
620 Hayden Lau, Jiaju Lin, Krishna Sri Ipsit Mantri, Ferdinand Mom, Atsushi Saito, Guangyu Song,
621 Xiangru Tang, Johan Wind, Stanisław Woźniak, Zhenyuan Zhang, Qinghua Zhou, Jian Zhu, and
622 Rui-Jie Zhu. RWKV: Reinventing RNNs for the transformer era. In Houda Bouamor, Juan
623 Pino, and Kalika Bali (eds.), *Findings of the Association for Computational Linguistics: EMNLP*
624 *2023*, pp. 14048–14077, Singapore, December 2023. Association for Computational Linguistics.
625 doi: 10.18653/v1/2023.findings-emnlp.936. URL <https://aclanthology.org/2023.findings-emnlp.936>.
626
- 627 Hao Peng, Nikolaos Pappas, Dani Yogatama, Roy Schwartz, Noah A. Smith, and Lingpeng
628 Kong. Random feature attention. In *9th International Conference on Learning Representations, ICLR 2021, Virtual Event, Austria, May 3-7, 2021*. OpenReview.net, 2021. URL
629 <https://openreview.net/forum?id=QtTKTdVrFBB>.
630
- 631 Zhen Qin and Yiran Zhong. Accelerating toeplitz neural network with constant-time inference
632 complexity. In *Proceedings of the 2023 Conference on Empirical Methods in Natural Language*
633 *Processing*. Association for Computational Linguistics, December 2023.
634
- 635 Zhen Qin, Xiaodong Han, Weixuan Sun, Dongxu Li, Lingpeng Kong, Nick Barnes, and Yiran Zhong.
636 The devil in linear transformer. In *Proceedings of the 2022 Conference on Empirical Methods*
637 *in Natural Language Processing*, pp. 7025–7041, Abu Dhabi, United Arab Emirates, December
638 2022a. Association for Computational Linguistics. URL <https://aclanthology.org/2022.emnlp-main.473>.
639
- 640 Zhen Qin, Weixuan Sun, Hui Deng, Dongxu Li, Yunshen Wei, Baohong Lv, Junjie Yan, Lingpeng
641 Kong, and Yiran Zhong. cosformer: Rethinking softmax in attention. In *International Confer-*
642 *ence on Learning Representations*, 2022b. URL <https://openreview.net/forum?id=B18CQrx2Up4>.
643
644
- 645 Zhen Qin, Xiaodong Han, Weixuan Sun, Bowen He, Dong Li, Dongxu Li, Yuchao Dai, Lingpeng
646 Kong, and Yiran Zhong. Toeplitz neural network for sequence modeling. In *The Eleventh*
647 *International Conference on Learning Representations*, 2023a. URL <https://openreview.net/forum?id=IxmWsm4xrua>.

- 648 Zhen Qin, Weixuan Sun, Kaiyue Lu, Hui Deng, Dongxu Li, Xiaodong Han, Yuchao Dai, Lingpeng
649 Kong, and Yiran Zhong. Linearized relative positional encoding. *Transactions on Machine*
650 *Learning Research*, 2023b.
- 651 Zhen Qin, Dong Li, Weigao Sun, Weixuan Sun, Xuyang Shen, Xiaodong Han, Yunshen Wei, Baohong
652 Lv, Xiao Luo, Yu Qiao, and Yiran Zhong. Transormer11m: A faster and better large language
653 model with improved transormer, 2024a.
- 654 Zhen Qin, Xuyang Shen, Weigao Sun, Dong Li, Stan Birchfield, Richard Hartley, and Yiran Zhong.
655 Unlocking the secrets of linear complexity sequence model from a unified perspective. *arXiv*
656 *preprint arXiv:2405.17383*, 2024b.
- 657 Zhen Qin, Songlin Yang, Weixuan Sun, Xuyang Shen, Dong Li, Weigao Sun, and Yiran Zhong.
658 Hgrn2: Gated linear rnns with state expansion. *arXiv preprint arXiv:2404.07904*, 2024c.
- 659 Zhen Qin, Songlin Yang, and Yiran Zhong. Hierarchically gated recurrent neural network for
660 sequence modeling. *Advances in Neural Information Processing Systems*, 36, 2024d.
- 661 Markus N. Rabe and Charles Staats. Self-attention does not need $o(n^2)$ memory. *CoRR*,
662 abs/2112.05682, 2021. URL <https://arxiv.org/abs/2112.05682>.
- 663 Samyam Rajbhandari, Jeff Rasley, Olatunji Ruwase, and Yuxiong He. Zero: Memory optimizations
664 toward training trillion parameter models, 2020.
- 665 Imanol Schlag and Jürgen Schmidhuber. Gated fast weights for associative retrieval. 2018.
- 666 Mohammad Shoeybi, Mostofa Patwary, Raul Puri, Patrick LeGresley, Jared Casper, and Bryan Catan-
667 zaro. Megatron-lm: Training multi-billion parameter language models using model parallelism.
668 *arXiv preprint arXiv:1909.08053*, 2019.
- 669 Jimmy T. H. Smith, Andrew Warrington, and Scott W. Linderman. Simplified state space layers
670 for sequence modeling. *CoRR*, abs/2208.04933, 2022. doi: 10.48550/arXiv.2208.04933. URL
671 <https://doi.org/10.48550/arXiv.2208.04933>.
- 672 Yutao Sun, Li Dong, Shaohan Huang, Shuming Ma, Yuqing Xia, Jilong Xue, Jianyong Wang, and
673 Furu Wei. Retentive network: A successor to transformer for large language models. *arXiv preprint*
674 *arXiv:2307.08621*, 2023.
- 675 Rajeev Thakur, Rolf Rabenseifner, and William Gropp. Optimization of collective communication
676 operations in mpich. *The International Journal of High Performance Computing Applications*, 19
677 (1):49–66, 2005.
- 678 Hugo Touvron, Thibaut Lavril, Gautier Izacard, Xavier Martinet, Marie-Anne Lachaux, Timothée
679 Lacroix, Baptiste Rozière, Naman Goyal, Eric Hambro, Faisal Azhar, Aurelien Rodriguez, Armand
680 Joulin, Edouard Grave, and Guillaume Lample. Llama: Open and efficient foundation language
681 models. *arXiv preprint arXiv:2302.13971*, 2023a.
- 682 Hugo Touvron, Louis Martin, Kevin Stone, Peter Albert, Amjad Almahairi, Yasmine Babaei, Nikolay
683 Bashlykov, Soumya Batra, Prajjwal Bhargava, Shruti Bhosale, Dan Bikel, Lukas Blecher, Cris-
684 tian Canton Ferrer, Moya Chen, Guillem Cucurull, David Esiobu, Jude Fernandes, Jeremy Fu,
685 Wenyan Fu, Brian Fuller, Cynthia Gao, Vedanuj Goswami, Naman Goyal, Anthony Hartshorn,
686 Saghar Hosseini, Rui Hou, Hakan Inan, Marcin Kardas, Viktor Kerkez, Madian Khabsa, Isabel
687 Kloumann, Artem Korenev, Punit Singh Koura, Marie-Anne Lachaux, Thibaut Lavril, Jenya Lee,
688 Diana Liskovich, Yinghai Lu, Yuning Mao, Xavier Martinet, Todor Mihaylov, Pushkar Mishra,
689 Igor Molybog, Yixin Nie, Andrew Poulton, Jeremy Reizenstein, Rashi Rungta, Kalyan Saladi,
690 Alan Schelten, Ruan Silva, Eric Michael Smith, Ranjan Subramanian, Xiaoqing Ellen Tan, Binh
691 Tang, Ross Taylor, Adina Williams, Jian Xiang Kuan, Puxin Xu, Zheng Yan, Iliyan Zarov, Yuchen
692 Zhang, Angela Fan, Melanie Kambadur, Sharan Narang, Aurelien Rodriguez, Robert Stojnic,
693 Sergey Edunov, and Thomas Scialom. Llama 2: Open foundation and fine-tuned chat models,
694 2023b.
- 695 Ashish Vaswani, Noam Shazeer, Niki Parmar, Jakob Uszkoreit, Llion Jones, Aidan N Gomez, Łukasz
696 Kaiser, and Illia Polosukhin. Attention is all you need. *Advances in neural information processing*
697 *systems*, 30, 2017.

702 Songlin Yang, Bailin Wang, Yikang Shen, Rameswar Panda, and Yoon Kim. Gated linear attention
703 transformers with hardware-efficient training. *arXiv preprint arXiv:2312.06635*, 2023.
704

705 Aohan Zeng, Xiao Liu, Zhengxiao Du, Zihan Wang, Hanyu Lai, Ming Ding, Zhuoyi Yang, Yifan Xu,
706 Wendi Zheng, Xiao Xia, et al. Glm-130b: An open bilingual pre-trained model. *arXiv preprint*
707 *arXiv:2210.02414*, 2022.

708 Susan Zhang, Stephen Roller, Naman Goyal, Mikel Artetxe, Moya Chen, Shuohui Chen, Christopher
709 Dewan, Mona Diab, Xian Li, Xi Victoria Lin, Todor Mihaylov, Myle Ott, Sam Shleifer, Kurt
710 Shuster, Daniel Simig, Punit Singh Koura, Anjali Sridhar, Tianlu Wang, and Luke Zettlemoyer.
711 Opt: Open pre-trained transformer language models, 2022.
712

713 Yanli Zhao, Andrew Gu, Rohan Varma, Liang Luo, Chien-Chin Huang, Min Xu, Less Wright, Hamid
714 Shojanazeri, Myle Ott, Sam Shleifer, et al. Pytorch fsdp: experiences on scaling fully sharded data
715 parallel. *arXiv preprint arXiv:2304.11277*, 2023.

716 Lin Zheng, Chong Wang, and Lingpeng Kong. Linear complexity randomized self-attention mecha-
717 nism. In *International Conference on Machine Learning*, pp. 27011–27041. PMLR, 2022.
718

719 Lin Zheng, Jianbo Yuan, Chong Wang, and Lingpeng Kong. Efficient attention via control variates.
720 In *International Conference on Learning Representations*, 2023. URL <https://openreview.net/forum?id=G-uNfHKrj46>.
721
722
723
724
725
726
727
728
729
730
731
732
733
734
735
736
737
738
739
740
741
742
743
744
745
746
747
748
749
750
751
752
753
754
755

A APPENDIX

A.1 BACKWARD PASS ALGORITHM

Algorithm 3 LASP Backward Pass

- 1: **Input:** Sequence Length N , Distributed world size W , sequence parallel size T , decay rate $\lambda \in \mathbb{R}^+$, $\mathbf{Q}_t, \mathbf{K}_t, \mathbf{V}_t, \mathbf{O}_t, \mathbf{dO}_t \in \mathbb{R}^{C \times d}$ for $t \in \{1, 2, \dots, T\}$.
 - 2: Obtain sub-sequence length (or chunk size) $C = N/T$.
 - 3: Initialize mask $\mathbf{M} \in \mathbb{R}^{C \times C}$, where $M_{ij} = \lambda^{i-j}$, if $i \geq j$, else $M_{ij} = 0$.
 - 4: Initialize $\mathbf{\Lambda} = \text{diag}\{\lambda, \lambda^2, \dots, \lambda^C\} \in \mathbb{R}^{C \times C}$.
 - 5: Initialize $\mathbf{dKV} = \mathbf{0} \in \mathbb{R}^{d \times d}$.
 - 6: **for** $t \in \{1, 2, \dots, T\}$ at rank $i \in \{1, 2, \dots, W\}$ in parallel **do**
 - 7: Compute $\mathbf{dQ}_{t,\text{intra}} = [(\mathbf{dO}_t \mathbf{V}_t^\top) \odot \mathbf{M}] \mathbf{K}_t$.
 - 8: Compute $\mathbf{dQ}_{t,\text{inter}} = \mathbf{\Lambda} \mathbf{dO}_t \mathbf{KV}_{t-1}^\top$.
 - 9: Compute $\mathbf{dK}_{t,\text{intra}} = [(\mathbf{dO}_t \mathbf{V}_t^\top) \odot \mathbf{M}]^\top \mathbf{Q}_t$.
 - 10: Compute $\mathbf{dV}_{t,\text{intra}} = [(\mathbf{Q}_t \mathbf{K}_t^\top) \odot \mathbf{M}]^\top \mathbf{dO}_t$.
 - 11: **end for**
 - 12: **for** $t \in \{T, \dots, 2, 1\}$ at rank $i \in \{W, \dots, 2, 1\}$ **do**
 - 13: Recv activation \mathbf{dKV}_{t+1} from rank $(i+1)$.
 - 14: Compute $\mathbf{dK}_{t,\text{inter}} = (\lambda^C \mathbf{\Lambda}^{-1} \mathbf{V}_t) \mathbf{dKV}_{t+1}^\top$.
 - 15: Compute $\mathbf{dV}_{t,\text{inter}} = (\lambda^C \mathbf{\Lambda}^{-1} \mathbf{K}_t) \mathbf{dKV}_{t+1}$.
 - 16: Load \mathbf{KV}_i as \mathbf{KV}_t on rank i .
 - 17: Combine intra- and inter-chunks of $\mathbf{dQ}_t, \mathbf{dK}_t, \mathbf{dV}_t$:

$$\begin{aligned} \mathbf{dQ}_t &= \mathbf{dQ}_{t,\text{intra}} + \mathbf{dQ}_{t,\text{inter}}, \\ \mathbf{dK}_t &= \mathbf{dK}_{t,\text{intra}} + \mathbf{dK}_{t,\text{inter}}, \\ \mathbf{dV}_t &= \mathbf{dV}_{t,\text{intra}} + \mathbf{dV}_{t,\text{inter}}. \end{aligned}$$
 - 18: Compute $\mathbf{dKV}_t = \lambda^C \mathbf{dKV}_{t+1} + (\mathbf{\Lambda} \mathbf{Q}_t)^\top \mathbf{dO}_t$.
 - 19: Send activation \mathbf{dKV}_t to rank i .
 - 20: **end for**
 - 21: return $\mathbf{dQ} = [\mathbf{dQ}_t], \mathbf{dK} = [\mathbf{dK}_t], \mathbf{dV} = [\mathbf{dV}_t]$, with $t \in \{1, 2, \dots, T\}$.
-

A.2 HARDWARE AND SOFTWARE

Hardware. Our experimental configuration involves a maximum of 16x DGX-A100 servers, each equipped with 8x A100 GPUs, these GPUs are interconnected through NVSwitch, ensuring an inter-GPU bandwidth of 600GBps. For inter-node communication, we employ RoCE (RDMA over Converged Ethernet) technology, utilizing 8 RoCE RDMA adapters in each server. This setup facilitates efficient inter-server communication with a bandwidth capacity of 800Gbps.

Software. Experiments are implemented in PyTorch 2.1.1 and Triton 2.0.0 with CUDA 11.7, cuDNN 8.0, and NCCL 2.14.3. Our algorithm is developed upon Metaseq and DeepSpeed.

A.3 EXPERIMENTAL SETUP

The training configuration is set with specific hyperparameters: a learning rate of 0.0005 to control the optimization step size, a cap of 50,000 updates to define the training duration, and a 2,000-update warmup period to stabilize early training by gradually adjusting the learning rate. Additionally, a weight decay rate of 0.01 is used for regularization to avoid over-fitting. The Adam optimizer, with beta values of 0.9 and 0.999, is chosen for managing the momentum and scaling of gradients, aiding in effective and stable training convergence. Different DDP backends, including PyTorch DDP (abbr. DDP), Legacy DDP, FSDP, ZeRO-series, are selected in experiments for cross-validation of compatibility with LASP.

A.4 GENERALIZATION OF LASP

Although the idea of LASP origins from the linear attention sequence modeling, we would like to demonstrate it is also applicable to other linear-complexity models.

We first define the following terms: Memory State $\mathbf{m}_t \in \mathbb{R}^{k \times d}$, Input State $\mathbf{i}_t \in \mathbb{R}^d$, Expand State $\mathbf{e}_t \in \mathbb{R}^k$, Oscillation State $\mathbf{o}_t \in \mathbb{R}^{k \times m}$, Shrink State $\mathbf{s}_t \in \mathbb{R}^k$ and write a general form of recurrent memory as (Qin et al., 2024b)

$$\mathbf{m}_t = \mathbf{o}_t \mathbf{m}_{t-1} + \mathbf{e}_t \mathbf{i}_t^\top. \quad (24)$$

which is general form of the recurrence form of Linear Attention in Eq. (5) with specified \mathbf{o}_t and \mathbf{e}_t :

$$\mathbf{k} \mathbf{v}_t = \lambda \mathbf{k} \mathbf{v}_{t-1} + \mathbf{k}_t \mathbf{v}_t^\top. \quad (25)$$

The design of LASP can be seamlessly applied to models which is able to be generally expressed by Eq. (24). These models include: S4 (Gu et al., 2022), S5 (Smith et al., 2022), DSS (Gupta et al., 2022), TNN (Qin et al., 2023a), Linear Attention (Katharopoulos et al., 2020), TNL (Qin et al., 2024a), RetNet (Sun et al., 2023), Mamba (Gu & Dao, 2023), RWKV-4 (Peng et al., 2023), Cosformer (Qin et al., 2022b), Lrpe (Qin et al., 2023b), GLA (Yang et al., 2023), GateLoop (Katsch, 2023), DUR (Mao, 2022), GFW (Schlag & Schmidhuber, 2018), HGRN (Qin et al., 2024d;c), and LRN (Martin & Cundy, 2018). We list all these models and their corresponding elements in Table 3.

Table 3: **Checklist for Typical Linear-Complexity Sequence Modeling Methods within the Defined General Form.** For each method, the following states are outlined: Input State, Expand State, Oscillation State, Shrink State, and Memory State. If the state is directly linked to the input sequence, the subscript i is emphasized. Note that we use $\mathbf{1}^{(k)} \in \mathbb{R}^k$, where $\mathbf{1}_j^{(k)} = 1$ for $j = 1, \dots, k$, and $\mathbf{J}^{(kd)} = \mathbf{1}^{(k)} \mathbf{1}^{(d)\top} \in \mathbb{R}^{k \times d}$.

Methods	Input \mathbf{i}_t	Expand \mathbf{e}_t	Oscillation \mathbf{o}_t	Shrink \mathbf{s}_t	Memory $k \times d$
S4	\mathbf{x}_t	\mathbf{B}	\mathbf{A}	\mathbf{C}	$k \times 1$
S5	\mathbf{x}_t	\mathbf{B}	\mathbf{A}	\mathbf{C}	$k \times d$
DSS	\mathbf{x}_t	\mathbf{B}	$\mathbf{a} \mathbf{1}_k^\top$	\mathbf{C}	$k \times d$
TNN	\mathbf{x}_t	\mathbf{B}	\mathbf{A}	\mathbf{C}	$k \times d$
Linear Attention	\mathbf{x}_t	\mathbf{B}_t	$\mathbf{J}^{(kd)}$	\mathbf{C}_t	$k \times d$
TNL/RetNet	\mathbf{x}_t	\mathbf{B}_t	$\lambda \mathbf{J}^{(k)}$	\mathbf{C}_t	$k \times d$
Mamba	\mathbf{x}_t	\mathbf{B}_t	\mathbf{A}_t	\mathbf{C}_t	$k \times d$
RWKV4	\mathbf{x}_t	$\exp(\mathbf{k}_t)$	$\exp(-w)$	\mathbf{C}_t	1×1
Cosformer	\mathbf{x}_t	\mathbf{B}_t	$\exp(i\theta) \mathbf{J}^{(kd)}$	\mathbf{C}_t	$k \times d$
LRPE	\mathbf{x}_t	\mathbf{B}_t	$\exp(i\theta) \mathbf{1}^{(d)\top}$	\mathbf{C}_t	$k \times d$
GLA/GateLoop	\mathbf{x}_t	\mathbf{B}_t	$\mathbf{g}_t \mathbf{1}_d^\top$	\mathbf{C}_t	$k \times d$
DUR/GFW	\mathbf{x}_t	\mathbf{B}_t	$\mathbf{g}_t \mathbf{g}_t^\top$	\mathbf{C}_t	$k \times d$
HGRN/LRN	\mathbf{x}_t	$1 - \mathbf{A}_t$	\mathbf{A}_t	\mathbf{C}_t	1×1

We also give the complete explanation for each modeling method as below.

S4. In S4, we obtain $u_t \in \mathbb{R}^d$ through linear projection from input x_t and $A \in \mathbb{R}^{k \times k}$, $B, C \in \mathbb{R}^{k \times 1}$ through SSM parameterization. The calculation is as follows:

$$m_t = A m_{t-1} + B u_t^\top, \quad y_t = m_t^\top C.$$

Note that the original definition of S4 is defined as a channel-wise mappings $f_i, i = 1, \dots, d$ of $\mathbb{R}^{n \times 1} \rightarrow \mathbb{R}^{n \times 1}$.

S5. The recurrence equation of S5 is the same as S4, with the only difference being the direct definition of the mapping $\mathbb{R}^{n \times d} \rightarrow \mathbb{R}^{n \times d}$ and $B, C \in \mathbb{R}^{k \times d}$.

DSS. The recurrence equation of DSS is same as S4/S5, with the only difference being the direct definition of the mapping $\mathbb{R}^{n \times d} \rightarrow \mathbb{R}^{n \times d}$ and $B, C \in \mathbb{R}^{k \times d}$, $A = \text{Diag} a \in \mathbb{R}^{k \times k}$.

TNN. According to (Qin & Zhong, 2023), TNN can be losslessly converted to SSM, where $C = J^{(kd)} \in \mathbb{R}^{k \times d}$, $B \in \mathbb{R}^{k \times d}$, $A = \text{Diag} \lambda_1, \dots, \lambda_k \in \mathbb{R}^{k \times k}$, get u_t from x_t through linear projection,

and it can be expressed as a recursive formula:

$$m_t = Am_{t-1} + Bu_t^\top, y_t = m_t^\top C.$$

Linear Attention. In Linear Attention, we obtain query $q_t \in \mathbb{R}^k$, key $k_t \in \mathbb{R}^k$, value $v_t \in \mathbb{R}^d$ from the input $x_t \in \mathbb{R}^d$ through linear projection, and recursively calculation is as follows:

$$kv_t = kv_{t-1} + k_tv_t^\top, y_t = kv_t^\top q_t.$$

TNL/RetNet. TNL/RetNet is a form of Linear Attention with exponential decay and the method for getting q_t, k_t, v_t are the same as those in Linear Attention, and lambda is a predefined parameter that cannot be learned. Its recursive calculation is:

$$kv_t = \lambda kv_{t-1} + k_tv_t^\top, y_t = kv_t^\top q_t.$$

Mamba. Mamba can be seen as a data-dependent S4. It uses the similar method to get u_t, A, B, C , the A_t, B_t, C_t are computed through x_t and A, B, C . Its recurrence equation is defined as:

$$m_t = A_t \odot m_{t-1} + B_t u_t^\top, y_t = m_t^\top C_t.$$

RWKV-4. In RWKV-4, we get r_t, k_t, v_t through linear projection from input x_t and w as a learnable weight. Ignoring the denominator of RWKV-4, the recurrence equation can be simplified as:

$$m_t = \exp(-w)m_{t-1} + \exp(k_t)v_t^\top, y_t = m_t^\top r_t.$$

Similar to S4, RWKV4 uses channel-wise mapping $f_i, i = 1, \dots, d$ of $\mathbb{R}^{n \times 1} \rightarrow \mathbb{R}^{n \times 1}$.

Cosformer. In Cosformer, we obtain query $q_t \in \mathbb{R}^k$, key $k_t \in \mathbb{R}^k$, value $v_t \in \mathbb{R}^d$ from the input $x_t \in \mathbb{R}^d$ and a prefined θ (not learnable). Then recursively calculate as follows:

$$kv_t = \exp(i\theta)kv_{t-1} + k_tv_t^\top, y_t = \text{Rel}[kv_t^\top]q_t.$$

Lrpe. In Lrpe, we obtain query $q_t \in \mathbb{R}^k$, key $k_t \in \mathbb{R}^k$, value $v_t \in \mathbb{R}^d$ from the input $x_t \in \mathbb{R}^d$, θ as a learnable weight and recursively calculate as follows:

$$kv_t = \Lambda kv_{t-1} + k_tv_t^\top, \Lambda = \text{diag}(\exp(i\theta_1), \dots, \exp(i\theta_k)), y_t = \text{Rel}[kv_t^\top]q_t.$$

GLA/GateLoop. In GLA/GateLoop, we obtain query $q_t \in \mathbb{R}^k$, key $k_t \in \mathbb{R}^k$, value $v_t \in \mathbb{R}^d$, decay $g_t \in \mathbb{R}^k$ from the input $x_t \in \mathbb{R}^d$ and recursively calculate as follows:

$$kv_t = \text{Diag}(g_t)kv_{t-1} + k_tv_t^\top, y_t = kv_t^\top q_t.$$

DUR/GFW In DUR/GFW, we obtain query $q_t \in \mathbb{R}^k$, key $k_t \in \mathbb{R}^k$, value $v_t \in \mathbb{R}^d$, decay $g_t \in \mathbb{R}^k, \bar{g}_t \in \mathbb{R}^d$ from the input $x_t \in \mathbb{R}^d$, and recursively calculate as follows:

$$kv_t = (g_t \bar{g}_t^\top) \odot kv_{t-1} + k_tv_t^\top, y_t = [kv_t^\top]q_t.$$

HGRN/LRN In HGRN/LRN, we obtain output gate $o_t \in \mathbb{R}^1$, forget gate $f_t \in \mathbb{R}^1$, input state $i_t \in \mathbb{R}^1$ from the input $x_t \in \mathbb{R}^1$, and recursively calculate as follows:

$$h_t = f_t \odot h_{t-1} + (1 - f_t)i_t^\top, y_t = h_t^\top o_t.$$

Similar to S4, HGRN/LRN use channel-wise mapping $f_i, i = 1, \dots, d$ of $\mathbb{R}^{n \times 1} \rightarrow \mathbb{R}^{n \times 1}$.

A.5 ADDITIONAL EXPERIMENT RESULTS

A.5.1 QUANTITATIVE SCALABILITY RESULTS

See Table 4 in next page.

Table 4: **Quantitative Scalability Results of LASP on Throughput (tokens/sec) and Memory Usage Per GPU (GB)**. Experiments are performed on TNL-1B, scaling sequence length from 2K to 4096K with a batch size of 1. Both DDP and FSDP backends are tested.

Sequence Length	GPUs	LASP + DDP		LASP + FSDP	
		Throughput	Memory	Throughput	Memory
2K	16	1893.3	22.5	1780.5	6.9
	32	1645.4	22.5	1671.2	6.6
	64	1639.7	22.5	1589.8	6.4
	128	1610.9	22.5	1566.2	6.2
4K	16	3686.9	22.5	3519.9	6.9
	32	3458.4	22.5	3304.4	6.6
	64	3245.3	22.5	3152.2	6.4
	128	3211.5	22.5	3075.7	6.2
8K	16	7076.9	22.5	6924.8	6.9
	32	7319.3	22.5	6472.9	6.6
	64	6869.1	22.5	6459.4	6.4
	128	6793.6	22.5	6398.4	6.2
16K	16	14036.8	22.5	13513.7	6.9
	32	14671.7	22.5	12978.9	6.6
	64	13828.6	22.5	12569.4	6.4
	128	13484.5	22.5	12184.5	6.2
32K	16	28354.6	24.4	25727.2	6.9
	32	27863.6	22.5	26646.4	6.6
	64	25275.9	22.5	25201.4	6.4
	128	24523.8	22.5	25638.9	6.2
64K	16	52993.1	28.3	48542.8	11
	32	53393.2	24.4	49648.6	6.6
	64	52024.2	22.5	49780.5	6.4
	128	51983.3	22.5	49833.3	6.2
128K	16	107682	36.1	84901.9	19
	32	93371.5	28.3	92718.8	10.6
	64	100046	24.4	96771.6	6.4
	128	95828.5	22.5	98975.9	6.2
256K	16	202057	51.7	136765	35.2
	32	190675	36.1	159326	18.7
	64	193341	28.3	170996	10.4
	128	187347.7	24.4	178628.4	6.3
512K	16	OOM	OOM	201791	67.5
	32	323596	51.7	250663	34.8
	64	304366	36.1	284803	18.5
	128	295128.5	28.3	298755	10.1
1024K	16	OOM	OOM	OOM	OOM
	32	OOM	OOM	358478	67.1
	64	523119	51.7	437728	34.6
	128	508383	36.1	459794	18.2
2048K	16	OOM	OOM	OOM	OOM
	32	OOM	OOM	OOM	OOM
	64	OOM	OOM	585326	66.9
	128	658432	51.7	597953	33.8
4096K	16	OOM	OOM	OOM	OOM
	32	OOM	OOM	OOM	OOM
	64	OOM	OOM	OOM	OOM
	128	OOM	OOM	792705	66.2

Table 5: **Ablation on System Engineering Optimizations Techniques Kernel Fusion and KV State Caching.** Experiments are conducted on TNL-1B model with a batch size of 2 and a sequence length of 8K, utilizing 2x A100 GPUs.

Kernel Fusion	KV State Cache	Throughput (tokens/s)	Memory Usage Per GPU (GB)
No	No	37684.4	49.5
Yes	No	44691.0	49.5
No	Yes	41179.6	49.7
Yes	Yes	45915.2	49.6

A.5.2 ABLATION STUDY ON SYSTEM ENGINEERING OPTIMIZATION

The system engineering optimizations techniques Kernel Fusion and KV State Caching are designed to enhance the execution efficiency of LASP in practice. We conduct ablation studies to further investigate their impact, the results of which are outlined in Table 5. We evaluate the training throughput and memory usage of a 1B TNL model with a batch size of 2 and a sequence length of 8K, utilizing 2x A100 GPUs. The results indicate that in these settings, Kernel Fusion and KV State Caching effectively boost the training throughput, with minor impact on memory usage.

A.5.3 ABLATION STUDY ON ACTIVATION REDUCING METHODS

LASP prominently reduces the activation memory usage during training process on per GPU, which is orthometric with another activation memory reducing method: activation checkpointing. Following we conduct ablation experiments on AC and LASP to reveal their performance on memory reduction. With pure DDP and FSDP, the maximum sequence lengths are able to train on 8 GPUs are 12K and 16K, respectively. Both AC and LASP can enlarge the maximum sequence length markedly, but encounters slightly throughput reduction. The distinction is the scaling-up performance of LASP is directly proportional to the number of GPUs used. By combining AC and LASP, we can obtain surprising maximum sequence lengths 496K and 768K on single node with using DDP and FSDP backends, respectively.

Table 6: **Ablation on Activation Reducing Methods.** Both DDP and FSDP backends are tested. A single node equipped with 8x A100 80G GPUs is used to train a TNL-1B model, still with a batch size of 1 for all experiments.

Method	Maximum Sequence Length	Throughput (tokens/sec)	Method	Maximum Sequence Length	Throughput (tokens/sec)
DDP	12K	131286.0	FSDP	16K	145303.6
DDP+AC	64K	117429.5	FSDP+AC	96K	114464.0
DDP+LASP	96K	126829.4	FSDP+LASP	120K	138598.8
DDP+AC+LASP	496K	100837.8	FSDP+AC+LASP	768K	106578.3

A.5.4 EVALUATION RESULTS ON DOWNSTREAM TASKS

We conduct an experiment with extended training duration of 300K steps (which consumes 40B tokens) to assess the performance of LASP, and its evaluation results on downstream tasks. Both TNL and Linear Transformer with 0.4B parameters are investigated. We evaluate the performance of the trained models on multiple downstream benchmarks, including PIQA, HellaSwag (HS), WinoGrande (WG), ARC-E, ARC-C, OBQA, and CSR-AVG. The results are presented in the Tables 7 and 8. LASP always shows comparable performances on convergence as well as downstream tasks.

1026
 1027
 1028
 1029
 1030
 1031
 1032
 1033
 1034
 1035
 1036
 1037
 1038
 1039
 1040
 1041
 1042
 1043
 1044
 1045
 1046
 1047
 1048
 1049
 1050
 1051
 1052
 1053
 1054
 1055
 1056
 1057
 1058
 1059
 1060
 1061
 1062
 1063
 1064
 1065
 1066
 1067
 1068
 1069
 1070
 1071
 1072
 1073
 1074
 1075
 1076
 1077
 1078
 1079

Table 7: **Convergence Results of LASP with Extended 300K steps.** Both TNL and Linear Transformer with 0.4B parameters are tested with a batch size of 2 and sequence length of 16K.

Model	Parameters	Steps	Method	Loss	PPL	Method	Loss	PPL
TNL	0.4B	300K	DDP	3.218	9.318	LASP+DDP	3.218	9.321
Linear Transformer	0.4B	300K	DDP	4.164	17.972	LASP+DDP	4.145	17.730

Table 8: **Evaluation Results on Downstream Tasks.** HS: HellaSwag, WG: WinoGrande. A higher score indicates better performance.

Model	Method	Tokens	PIQA	HS	WG	ARC-E	ARC-C	OBQA	CSR-AVG
TNL	DDP	40B	55.71	28.21	51.30	28.87	23.72	26.00	35.64
TNL	LASP+DDP	40B	54.30	28.17	51.54	31.27	24.06	29.60	36.49
Linear Transformer	DDP	40B	52.18	25.68	49.80	26.81	25.60	26.40	34.93
Linear Transformer	LASP+DDP	40B	52.18	26.07	49.25	26.22	26.71	27.00	35.44